

**Direct Observation of Dynamically Localized Quantum Optical States**Ze-Kun Jiang<sup>1,2</sup>, Ruo-Jing Ren<sup>1,2</sup>, Yi-Jun Chang<sup>1,2</sup>, Wen-Hao Zhou<sup>1,2</sup>, Yong-Heng Lu<sup>1,2</sup>, Xiao-Wei Wang<sup>1,2</sup>,  
Li Wang<sup>1,2</sup>, Chang-Shun Wang<sup>3,\*</sup>, Alexander S. Solntsev<sup>4,†</sup>, and Xian-Min Jin<sup>1,2,5,‡</sup><sup>1</sup>*Center for Integrated Quantum Information Technologies (IQIT), School of Physics and Astronomy  
and State Key Laboratory of Advanced Optical Communication Systems and Networks,  
Shanghai Jiao Tong University, Shanghai 200240, China*<sup>2</sup>*CAS Center for Excellence and Synergetic Innovation Center in Quantum Information and Quantum Physics,  
University of Science and Technology of China, Hefei, Anhui 230026, China*<sup>3</sup>*School of Physics and Astronomy and State Key Laboratory of Advanced Optical Communication Systems and Networks,  
Shanghai Jiao Tong University, Shanghai 200240, China*<sup>4</sup>*School of Mathematical and Physical Sciences, University of Technology Sydney, Ultimo, New South Wales, Australia*<sup>5</sup>*TuringQ Co., Ltd., Shanghai 200240, China*

(Received 20 March 2022; accepted 31 August 2022; published 20 October 2022)

Quantum-correlated biphoton states play an important role in quantum communication and processing, especially considering the recent advances in integrated photonics. However, it remains a challenge to flexibly transport quantum states on a chip, when dealing with large-scale sophisticated photonic designs. The equivalence between certain aspects of quantum optics and solid-state physics makes it possible to utilize a range of powerful approaches in photonics, including topologically protected boundary states, graphene edge states, and dynamic localization. Optical dynamic localization allows efficient protection of classical signals in photonic systems by implementing an analogue of an external alternating electric field. Here, we report on the observation of dynamic localization for quantum-correlated biphotons, including both the generation and the propagation aspects. As a platform, we use sinusoidal waveguide arrays with cubic nonlinearity. We record biphoton coincidence count rates as evidence of robust generation of biphotons and demonstrate the dynamic localization features in both spatial and temporal space by analyzing the quantum correlation of biphotons at the output of the waveguide array. Experimental results demonstrate that various dynamic modulation parameters are effective in protecting quantum states without introducing complex topologies. Our Letter opens new avenues for studying complex physical processes using photonic chips and provides an alternative mechanism of protecting communication channels and nonclassical quantum sources in large-scale integrated quantum optics.

DOI: [10.1103/PhysRevLett.129.173602](https://doi.org/10.1103/PhysRevLett.129.173602)

Photons have been widely used as qubits in photonic platforms to implement various quantum protocols, such as quantum walks [1–4], boson sampling [5], and quantum fast hitting [6]. Photonics also benefited significantly from the equivalence between certain aspects of solid-state physics and optics [7]. In this vein, many optical analogies are proposed to simulate particle dynamics [8,9], such as optical solitons [10–13], Anderson localization [14,15], an optical dimerized-type chain resembling the Su-Schrieffer-Heeger (SSH) model [16–20], Bloch oscillations [21,22], and dynamic localization (DL) [23–27]. The extraordinary nonclassical behavior of particles in these special examples is difficult to observe in the solid state due to sophisticated interactions in matter. Optics, however, provides a platform for the demonstration of these effects, and also benefits from utilizing them to enhance photonic designs and their functionality [8].

Dynamic localization was originally introduced by Dunlap and Kenkre [28], where they predicted a periodical

suppression of the broadening of the electron wave packet synchronized with the alternating oscillation of an external potential. Experimental observation of optical DL has been reported in sinusoidally curved waveguide arrays [25–27], where the curvature acts as an external driving force by analogy with the original model. Optical DL effect shows good correspondence with diffraction cancellation [29,30] and self-collimation [31,32], and provides a new strategy for the manipulation of optical signals on a chip.

A range of quantum states, especially multiparticle implementations, can offer unique advantages in quantum algorithms. For example, driven quantum walks within a nonlinear lattice can perform a faster search algorithm than classical ones [33]. Thus studies of behaviors of quantum states in waveguide arrays, most commonly generated via spontaneous parametric down-conversion (SPDC) [34,35] and spontaneous four wave mixing (SFWM) [20,36,37], will further promote the development of quantum photonics.

Although several demonstrations of optical DL in different systems have been reported, the study of DL effects on quantum states remained unresolved.

On-chip generation of quantum states in nonlinear waveguides is essential for a range of quantum devices [38,39]. The design of various components in future quantum photonic circuits will be significantly influenced by the consideration of geometry, footprint, and crosstalk between the channels. As the photonic chip scales increase, the integration of protected nonclassical quantum sources and the crosstalk-free communication channels become ever more important. However, most protection mechanisms require a large number of auxiliary waveguides, which greatly limits the integration of photonic chips.

In this Letter, we report on the observation of dynamic localization for biphoton quantum states in sinusoidal waveguide arrays. We theoretically and experimentally investigate the dynamics of correlated biphoton states generated within the array via the SFWM process supported by cubic nonlinearity. We record coincidence count rates that are 3 times higher in curved arrays than in the straight array as evidence of robust generation of biphoton states. We further verify the DL in both spatial and temporal space by measuring the cross-correlation  $g_{s,i}^{(2)}(0)$  with a minimum value of 239.19 and correlation matrices in which only the central peak attains a nonzero value [40]. In contrast, the crosstalk between waveguides in the straight array reduces the maximum value of the correlations by a factor of 5 and results in strong correlations between the photons from different waveguides. Our results demonstrate this dynamic modulation as a quantum state protection mechanism that allows us the freedom to design the modulation parameters without introducing defect states. We also discuss the case of off-chip injection of biphoton states to demonstrate the power of this mechanism in a passive device in section C of the Supplemental Material [41].

In our experiment, the waveguides are set to periodically bend in the ( $x$ - $z$ ) plane along the propagation direction  $z$ , which can be mathematically characterized by a profile function  $x_0(z)$ . The effective two-dimensional wave equation describing beam propagation reads [8,9,25,27,42]

$$i\tilde{\lambda} \frac{\partial \psi}{\partial z} = -\frac{\tilde{\lambda}^2}{2n_s} \frac{\partial^2 \psi}{\partial x^2} + \Delta n(x - x_0(z))\psi \quad (1)$$

where  $\psi$  is the beam envelope function,  $\tilde{\lambda} \equiv \lambda/(2\pi)$  is the reduced wavelength,  $\Delta n(x) \simeq n_s - n(x)$  is the effective refractive index variance forming the waveguides,  $n(x)$  is effective refractive index of the array with period  $d$  [ $n(x+d) = n(x)$ ], and  $n_s$  is the substrate refractive index.

For single-mode waveguides, light transport in the lattice can be predicted by coupled-mode theory (CMT) using the nearest-neighbor tight-binding approximation and lowest

Bloch band excitation assumption. Equation (1) is then derived as [25,27,43]

$$-i \frac{da_n}{dz} = iC \exp[-i\dot{x}_0(z)]a_{n+1} + iC \exp[i\dot{x}_0(z)]a_{n-1} \quad (2)$$

where  $a_n$  is the field amplitude in the  $n$ th waveguide, and  $C = \text{Re}[C]$  is the coupling constant in a lossless waveguide array. The periodic revivals of the field amplitude  $a_n$  are referred to as the optical DL effect, i.e.,  $a_n(z') = a_n(0)$  with  $z' = \Lambda, 2\Lambda, 3\Lambda, \dots$ . In the case of sinusoidal waveguide arrays, the DL condition can be deduced to  $J_m(\zeta) = 0$  with  $J_m$  being the  $m$ th order Bessel function and  $\zeta$  satisfying the condition  $\zeta = 4\pi^2 n_s dA/\Lambda\lambda$  [25,27,44].

The evolution of the correlated photon pairs generated via SFWM can be characterized by the biphoton wave function  $\psi_{n_s, n_i}(z)$ . Under the nondepleting pump assumption, the linear propagation of the pump light is independent of the generation of biphotons. The dynamic equation for biphoton states can be decoupled from the dynamic equation of the pump light [37]:

$$\begin{aligned} d\psi_{n_s, n_i}(z)/dz = & iC_s \exp[i\dot{x}_0(z)]\psi_{n_s-1, n_i}(z) \\ & + iC_i \exp[i\dot{x}_0(z)]\psi_{n_s, n_i-1}(z) \\ & + iC_s \exp[-i\dot{x}_0(z)]\psi_{n_s+1, n_i}(z) \\ & + iC_i \exp[-i\dot{x}_0(z)]\psi_{n_s, n_i+1}(z) \\ & + i\Delta\beta^{(0)}\psi_{n_s, n_i} + \gamma a_{n_s}^{(p)}(z)a_{n_i}^{(p)}(z)\delta_{n_s, n_i}. \end{aligned} \quad (3)$$

Here  $n_s$  and  $n_i$  are the waveguide numbers describing the position of the signal and idler photons.  $C_s$ ,  $C_i$  are coupling constants of signal and idler photons [41], and  $a_n^{(p)}$  is the pump amplitude in the  $n$ th waveguide.  $\Delta\beta^{(0)} = 2\beta_p - \beta_s - \beta_i$  and  $\gamma$  refer to linear four-wave mixing phase mismatch in a single waveguide and nonlinear constant, respectively.

The cross-correlation  $g_{n_s, n_i}^{(2)}(0)$  between signal and idler in the  $n_s$ ,  $n_i$ th waveguide is obtained as  $\Gamma_{n_s, n_i} = |\psi_{n_s, n_i}(z)|^2$ .

Three groups of waveguide arrays with different modulation parameters, termed array (1), array (2), and array (3), are inscribed by means of femtosecond laser direct writing in a silica chip with  $\chi^{(3)}$  nonlinearity [36,41,45]. The overview of our chip is shown in Fig. 1(a). The total length of the chip is  $L_0 = 19.5$  mm. Each array includes a set of 25 identical waveguides with the same propagation length  $L = 19$  mm evenly distributed by a spacing  $d = 9 \mu\text{m}$  and labeled from  $n = -12$  to  $n = 12$ . Waveguides with  $n = -12, -6, 0, 6, 12$  are lengthened by 0.5 mm for the convenience of light injection. Without the loss of generality, the main text only discusses the case of light propagation in an infinite array, where the pump light is injected from waveguides with  $n = -6, 0, 6$  (which are termed as port 1, port 2, and port 3). For more discussion of the boundary waveguides see section B of the Supplemental Material [41]. Arrays (2) and (3) are

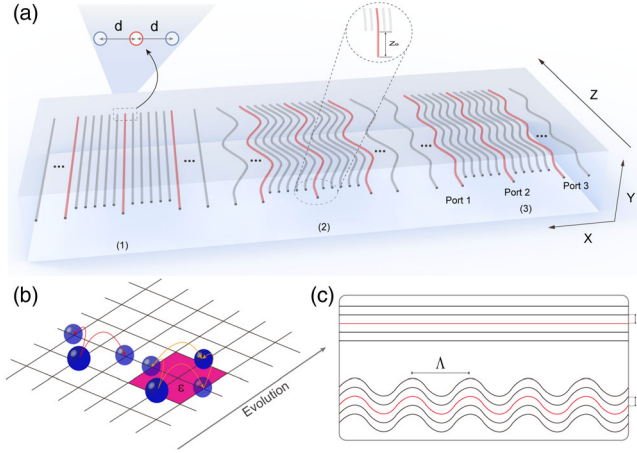


FIG. 1. Schematic of the on-chip dynamic protection system and the physical demonstration of dynamic localization. (a) The lattice contains three waveguide arrays with different modulation periods  $\Lambda$  and the corresponding amplitude  $A$  fulfilling the DL condition. Straight waveguides correspond to  $\Lambda = \infty$  and  $A = 0$ . Each group includes 25 uniformly fabricated waveguides with the same propagation length  $L = 19$  mm. The separation distances  $d = 9 \mu\text{m}$  between the adjacent waveguides are equal, and waveguides with  $n = -12, -6, 0, 6, 12$  are lengthened by  $z_0 = 0.5$  mm. We refer to the waveguides with  $n = -6, 0, 6$  (red colored) as ports 1, 2, 3, respectively. (b) Schematic of DL effect on electrons, in analogy with optical lattices. The localized particle will return to its initial state after a period of motion if a periodically oscillated electric potential field  $\mathcal{E}$  exists, otherwise the particle wave packet will keep broadening. (c) Optical analogy for the motion of a particle. The curvature of waveguides provides the optical equivalent of  $\mathcal{E}$ . The red color represents the light being injected into the certain waveguide.

modulated with periods  $\Lambda = L/2$  and  $\Lambda = L/3$  and the corresponding amplitudes  $A = \zeta \Lambda \lambda / 4\pi^2 n_s d$  that satisfy the DL condition, respectively, to observe the effect of different modulation parameters. Straight array (1) is equivalent to a specially modulated array with period  $\Lambda = \infty$  and amplitude  $A = 0$  corresponding to the case where the ac field is absent. The transverse shift function of each port now reads

$$x_0(z) = \begin{cases} 0, & \text{if } 0 \leq z < z_0 \\ A \left\{ \cos \left[ \frac{2\pi(z-z_0)}{\Lambda} \right] - 1 \right\}, & \text{if } z_0 \leq z \leq L_0 \end{cases} \quad (4)$$

with  $z_0 = 0.5$  mm.

The wavelength of the pump light is 780 nm and we choose the DL parameter  $\zeta$  to be 2.405, being the first root of the zero-order Bessel function. The propagation of the pump light is visually demonstrated based on the CMT calculation in the left panel of Fig. 2(b). Light in sinusoidal arrays is predicted to be localized at the output, whereas in the straight array it should spread linearly with respect to the propagation distance  $z$ .

For verification of the DL effect, we record the output intensity distribution of the pump light injected from port 2

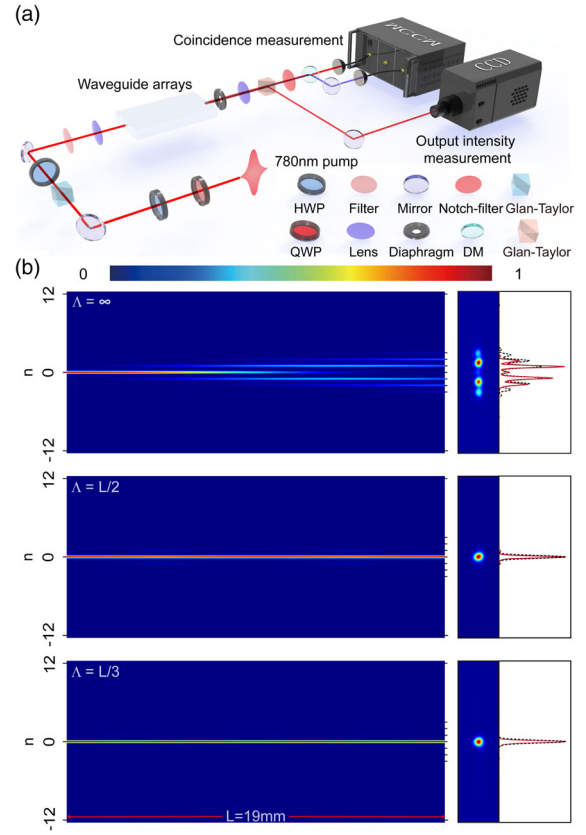


FIG. 2. Experimental setup and visualization of pump light dynamics. (a) Experimental setup for the measurement of the correlated biphotons. (b) Visualized dynamics of the pump light in different arrays. We take the pump light in port 2 as a representative. Left: evolution of the pump light predicted by CMT. Right: experimentally measured 2D output intensity pattern and the corresponding cross section. Red solid line: experimental data. Dashed line: numerical data based on CMT calculation.  $n$  refers to the waveguide number.

of each array. The experimental layout is schematically depicted in Fig. 2(a). By moving the chip placed on a three-dimensional translating stage, we can switch the injection of the pump light between different arrays and ports. Intense pump pulses from a mode-locked femtosecond laser at a wavelength of 780 nm are vertically polarized by a combination of wave plates and Glan-Taylor polarizer and injected into the chip, which is then reflected to a CCD camera by another Glan-Taylor polarizer at the chip's output for intensity measurement. Numerical and experimental data are normalized to their local maxima and collated in the right panel of Fig. 2(b) for comparison. Clear contrast reveals DL effects in sinusoidal arrays (2) and (3) after two and three periods of Bloch oscillations, respectively, as well as a strong diffusion in the array (1).

We further investigate the behavior of biphoton states in different arrays. Correlated photon pairs are generated in cubic nonlinear waveguides via the SFWM process. The phase-matching condition determines the spectral features

of photon pairs between different waveguides, thus the protection of it is important to improve the scalability of on-chip integrated quantum sources [36,41,45].

We inject the pump light into ports 1, 2, and 3 of each array, respectively, and collect coincidence count rates between signal and idler photons from the pumped waveguides. Residual pump light is filtered by a notch filter. Signal and idler photons are separated by a dichroic mirror (DM) and coupled to single photon avalanche diodes (SPADs) via two couplers [41]. The SPADs are connected to a homemade multichannel coincidence module (MCCM). We detect individual photons in each channel and record their arrival times to further calculate their coincidence count rate with an accuracy of 2 ns. Results are depicted in Fig. 3(a). The coincidence count rates witness the temporal correlations between signal and idler photons and are regarded as an important criterion for evaluating the performance of chip-scale quantum sources [38]. Higher count rates in the sinusoidal arrays suggests that the biphotons are protected by the localization effect. The dynamic modulation suppressed the broadening of the biphoton wave packet, which is discussed in section C of the Supplemental Material [41]. We also measure the wavelengths of signal and idler photons from each port of each array, as shown in Fig. 3(b). The deviation of the central wavelength is within  $\pm 2$  nm even with the existence of a transverse shift, which implies that this protection mechanism is still valid for the phase-matching in SFWM.

It is notable that the coincidence count rate cannot adequately address the quantum correlation property within the photon pairs. Cross-correlation  $g_{s,i}^{(2)}(0)$  described by Eq. (5) is introduced to quantify the nonclassical feature of biphotons [46,47]. A higher value of  $g_{s,i}^{(2)}(0)$  suggests that signal and idler photons are more likely to be bunched together, which ensures that they are indistinguishable in the degree of time and thus allows the potential establishment of entanglement [40].

$$g_{s,i}^{(2)}(0) = \frac{\langle \hat{a}_s^\dagger \hat{a}_i^\dagger \hat{a}_i \hat{a}_s \rangle}{\langle \hat{a}_s^\dagger \hat{a}_s \rangle \langle \hat{a}_i^\dagger \hat{a}_i \rangle} \quad (5)$$

We measure  $g_{s,i}^{(2)}(0)$  at the output of each pumped port, see Fig. 3(b). The  $g_{s,i}^{(2)}(0)$  has a minimum value of 239.19 in sinusoidal arrays (2) and (3) which is almost 5 times greater than the maximum value of 48.72 in the straight array (1). This large disparity implies that the sinusoidal arrays can effectively protect the quantum correlation between paired photons, which is reminiscent of the localization effect in the temporal domain. Similar results for both arrays demonstrate the equivalence between different modulation parameters. Considering the absence of topological states due to symmetry between the bulk waveguides (with  $n \neq \pm 12$ ), the uniformity of  $g_{s,i}^{(2)}(0)$  values across all three ports in the same array implies that the quantum correlation

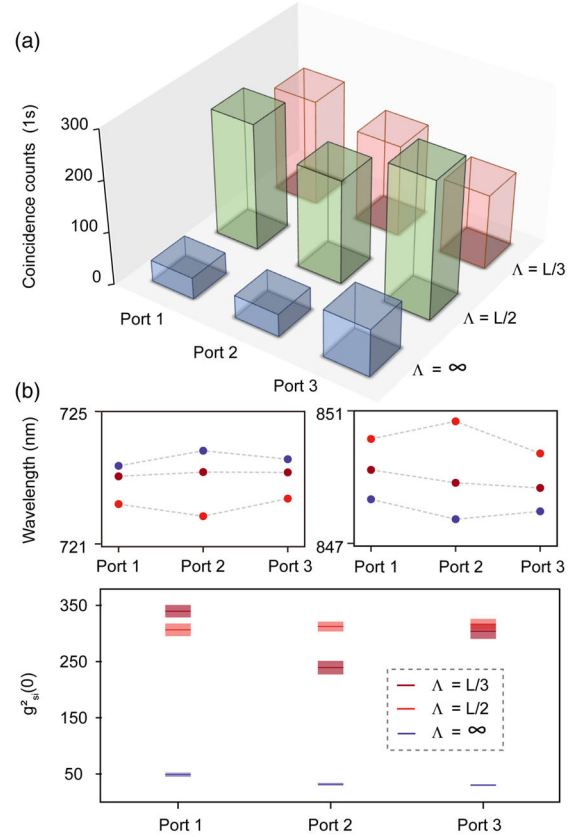


FIG. 3. Experimental verification of the protective mechanism for quantum biphoton states. (a) The coincidence count rate is recorded as evidence of the generation of biphoton states. Higher count rates in curved waveguide arrays indicate the DL of photon pairs under periodically changed potential. (b) The wavelengths of signal (left) and idler (right) photons are shown in the first row. The deviation of the central wavelength from the average wavelength is within  $\pm 2$  nm, indicating that the phase-matching process is effectively protected. The values for correlations  $g_{s,i}^{(2)}(0)$  are measured at the output of each port in three arrays. The shaded part corresponds to the error bars. Different colors refer to arrays with different modulation parameters as shown in the legend.

is universally protected among all bulk waveguides. For boundary waveguides with  $n = \pm 12$ , the symmetry breaking can lead to different behavior in the biphoton generation process, which will be discussed in section B of the Supplemental Material [41].

We next measure the cross-correlation matrices between port 2 and its most adjacent waveguides  $g_{n_s, n_i}^{(2)}(0)$ . The results are compared with CMT calculation (Fig. 4). Given that port 2 is designated as  $n = 0$ ,  $n_s$ , and  $n_i$  should be  $-1, 0, 1$ . We place the couplers on a high-precision translation stage to pick up the photons from different waveguides and block unwanted photons from waveguides with  $|n| > 1$  (see section D of the Supplemental Material [41]). Diffusion of the biphoton wave packet in the straight array (1) leads to substantial but varying degrees of

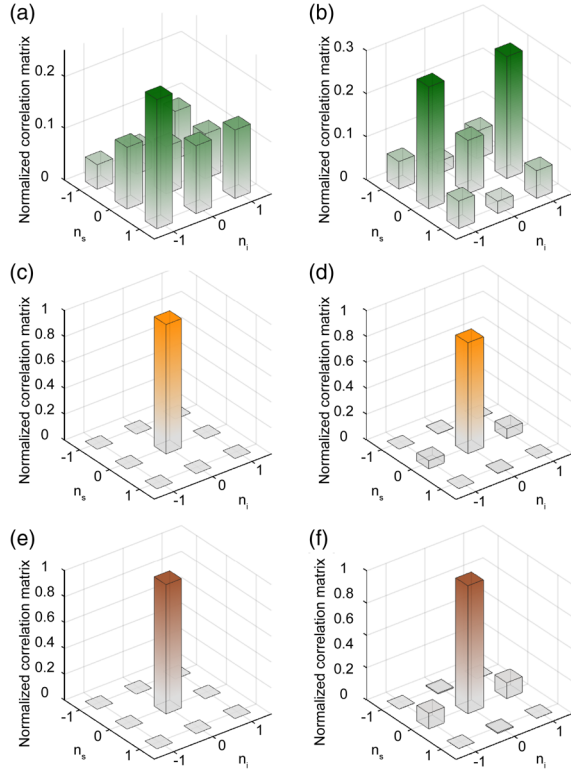


FIG. 4. Correlation matrices as an assessment of the DL effect on quantum biphoton states. Correlation matrices  $g_{n_s, n_i}^{(2)}(0)$  show the quantum correlation between port 2 and its adjacent waveguides. The left column shows the experimental measured matrices compared with the simulation results shown in the right column. Here  $n_s, n_i = -1, 0, 1$  refer to the waveguide numbers describing the position of signal and idler photons. Top to bottom: corresponding to array (1), (2), and (3), respectively.

correlation between signal and idler photons from the distinct waveguides, suggesting severe crosstalk. Considering the difference in coupling constants due to the different wavelengths of signal and idler photons, the photons collected from each waveguide come from different waveguides and will lead to a decrease in the  $g_{s,i}^{(2)}(0)$  value in the straight array (1). In contrast, the correlation is predicted to become strongest when paired photons are detected at the output of the pumped waveguide ( $n = 0$ ) in sinusoidal arrays (2) and (3). Experimentally we measure and find that only photon pairs from the central waveguide have quantum correlations. This is understandable because it is difficult to pick up photons from waveguides with  $n \neq 0$  due to the spatial DL effect and therefore we cannot observe their correlations in this experiment. This demonstration shows that the wave packet broadening of biphoton states is strongly suppressed in sinusoidal arrays. The experimentally measured correlation matrix of the straight array suggests more severe crosstalk than expected due to the fluctuation of the coupling constants introduced in the fabrication process; however, the quantum correlation

property of correlated photon pairs can still be effectively protected by this dynamic modulation.

In summary, we experimentally observe the DL effect on correlated photon pairs in the spatial and temporal domain in sinusoidally curved waveguide arrays. The dynamic modulation of the waveguides has an indirect effect on the generation of quantum states by localizing the pump light, and directly regulates the evolution of correlated photon pairs. By introducing nonlinearity into the waveguides, our Letter may further promote the use of the correspondence between solid state and optical systems to improve experimental accessibility, and provide a new vision of observing complicated physical processes [48].

From the perspective of practical applications, our results demonstrate a protective mechanism against crosstalk and diffraction, which is effective for both the generation and the propagation of quantum states. This mechanism eliminates the need to introduce sophisticated topologies, thus allowing more freedom in designing photonic circuits with different geometries and further improving the integration. We believe that it will open new opportunities in the development of large scalable integrated quantum photonics [49].

The authors thank Jian-Wei Pan for helpful discussions. This research is supported by the National Key R&D Program of China (2019YFA0308700, 2019YFA0706302 and 2017YFA0303700); National Natural Science Foundation of China (NSFC) (11904229, 61734005, 11761141014, 11690033, 92050116); Science and Technology Commission of Shanghai Municipality (STCSM) (20JC1416300, 2019SHZDZX01); Shanghai Municipal Education Commission (SMEC) (2017-01-07-00-02-E00049); China Postdoctoral Science Foundation (2020M671091). Australian Research Council (DE180100070); X.-M. J. acknowledges additional support from a Shanghai talent program and support from Zhiyuan Innovative Research Center of Shanghai Jiao Tong University.

Z.-K. J. and R.-J. R. contributed equally to this work.

\*cswang@sju.edu.cn

†alexander.solntsev@uts.edu.au

‡xianmin.jin@sju.edu.cn

- [1] A. Schreiber, K. N. Cassemiro, V. Potoček, A. Gábris, P. J. Mosley, E. Andersson, I. Jex, and C. Silberhorn, *Phys. Rev. Lett.* **104**, 050502 (2010).
- [2] L. Sansoni, F. Sciarrino, G. Vallone, P. Mataloni, A. Crespi, R. Ramponi, and R. Osellame, *Phys. Rev. Lett.* **108**, 010502 (2012).
- [3] A. Peruzzo, M. Lobino, J. C. F. Matthews, N. Matsuda, A. Politi, K. Poulios, X.-Q. Zhou, Y. Lahini, N. Ismail, K. W. Whoff, Y. Bromberg, Y. Silberberg, M. G. Thompson, and J. L. O'Brien, *Science* **329**, 1500 (2010).

- [4] H. Tang, X.-F. Lin, Z. Feng, J.-Y. Chen, J. Gao, K. Sun, C.-Y. Wang, P.-C. Lai, X.-Y. Xu, Y. Wang, L.-F. Qiao, A.-L. Yang, and X.-M. Jin, *Sci. Adv.* **4**, eaat3174 (2018).
- [5] J. B. Spring, B. J. Metcalf, P. C. Humphreys, W. S. Kolthammer, X.-M. Jin, M. Barbieri, A. Datta, N. Thomas-Peter, N. K. Langford, D. Kundys, J. C. Gates, B. J. Smith, P. G. R. Smith, and I. A. Walmsley, *Science* **339**, 798 (2013).
- [6] H. Tang, C. Di Franco, Z.-Y. Shi, T.-S. He, Z. Feng, J. Gao, K. Sun, Z.-M. Li, Z.-Q. Jiao, T.-Y. Wang *et al.*, *Nat. Photonics* **12**, 754 (2018).
- [7] S. Longhi, *Opt. Lett.* **35**, 235 (2010).
- [8] S. Longhi, *Laser Photonics Rev.* **3**, 243 (2009).
- [9] D. N. Christodoulides, F. Lederer, and Y. Silberberg, *Nature (London)* **424**, 817 (2003).
- [10] M. J. Ablowitz and Z. H. Musslimani, *Phys. Rev. Lett.* **87**, 254102 (2001).
- [11] M. J. Ablowitz and Z. H. Musslimani, *Physica (Amsterdam)* **184D**, 276 (2003).
- [12] K. Krupa, K. Nithyanandan, U. Andral, P. Tchofo-Dinda, and P. Grelu, *Phys. Rev. Lett.* **118**, 243901 (2017).
- [13] G. Herink, F. Kurtz, B. Jalali, D. R. Solli, and C. Ropers, *Science* **356**, 50 (2017).
- [14] M. Segev, Y. Silberberg, and D. N. Christodoulides, *Nat. Photonics* **7**, 197 (2013).
- [15] L. Martin, G. D. Giuseppe, A. Perez-Leija, R. Keil, F. Dreisow, M. Heinrich, S. Nolte, A. Szameit, A. F. Abouraddy, D. N. Christodoulides, and B. E. A. Saleh, *Opt. Express* **19**, 13636 (2011).
- [16] J. K. Asbóth, L. Oroszlány, and A. Pályi, *Lect. Notes Phys.* **919**, 166 (2016).
- [17] W. P. Su, J. R. Schrieffer, and A. J. Heeger, *Phys. Rev. Lett.* **42**, 1698 (1979).
- [18] Z.-Q. Jiao, S. Longhi, X.-W. Wang, J. Gao, W.-H. Zhou, Y. Wang, Y.-X. Fu, L. Wang, R.-J. Ren, L.-F. Qiao, and X.-M. Jin, *Phys. Rev. Lett.* **127**, 147401 (2021).
- [19] R.-J. Ren, Y.-H. Lu, Z.-K. Jiang, J. Gao, W.-H. Zhou, Y. Wang, Z.-Q. Jiao, X.-W. Wang, A. S. Solntsev, and X.-M. Jin, *arXiv:2106.07425*.
- [20] A. Blanco-Redondo, B. Bell, D. Oren, B. J. Eggleton, and M. Segev, *Science* **362**, 568 (2018).
- [21] F. Bloch, *Z. Phys.* **52**, 555 (1929).
- [22] G. H. Wannier, *Rev. Mod. Phys.* **34**, 645 (1962).
- [23] T. Pertsch, P. Dannberg, W. Elflein, A. Bräuer, and F. Lederer, *Phys. Rev. Lett.* **83**, 4752 (1999).
- [24] R. Morandotti, U. Peschel, J. S. Aitchison, H. S. Eisenberg, and Y. Silberberg, *Phys. Rev. Lett.* **83**, 4756 (1999).
- [25] S. Longhi, M. Marangoni, M. Lobino, R. Ramponi, P. Laporta, E. Cianci, and V. Foglietti, *Phys. Rev. Lett.* **96**, 243901 (2006).
- [26] A. Szameit, I. L. Garanovich, M. Heinrich, A. A. Sukhorukov, F. Dreisow, T. Pertsch, S. Nolte, A. Tünnermann, S. Longhi, and Y. S. Kivshar, *Phys. Rev. Lett.* **104**, 223903 (2010).
- [27] S. Longhi, *Opt. Lett.* **30**, 2137 (2005).
- [28] D. H. Dunlap and V. M. Kenkre, *Phys. Rev. B* **34**, 3625 (1986).
- [29] H. S. Eisenberg, Y. Silberberg, R. Morandotti, and J. S. Aitchison, *Phys. Rev. Lett.* **85**, 1863 (2000).
- [30] T. Pertsch, T. Zentgraf, U. Peschel, A. Bräuer, and F. Lederer, *Phys. Rev. Lett.* **88**, 093901 (2002).
- [31] H. Kosaka, T. Kawashima, A. Tomita, M. Notomi, T. Tamamura, T. Sato, and S. Kawakami, *Appl. Phys. Lett.* **74**, 1212 (1999).
- [32] X. Yu and S. Fan, *Appl. Phys. Lett.* **83**, 3251 (2003).
- [33] C. S. Hamilton, R. Kruse, L. Sansoni, C. Silberhorn, and I. Jex, *Phys. Rev. Lett.* **113**, 083602 (2014).
- [34] D. Leykam, A. S. Solntsev, A. A. Sukhorukov, and A. S. Desyatnikov, *Phys. Rev. A* **92**, 033815 (2015).
- [35] A. S. Solntsev, A. A. Sukhorukov, D. N. Neshev, and Y. S. Kivshar, *Phys. Rev. Lett.* **108**, 023601 (2012).
- [36] R.-J. Ren, J. Gao, W.-H. Zhou, Z.-Q. Jiao, L.-F. Qiao, X.-W. Wang, and X.-M. Jin, *Phys. Rev. Applied* **16**, 054026 (2021).
- [37] A. S. Solntsev, A. A. Sukhorukov, D. N. Neshev, and Y. S. Kivshar, *Opt. Express* **20**, 27441 (2012).
- [38] G. Moody, L. Chang, T. J. Steiner, and J. E. Bowers, *AVS Quantum Sci.* **2**, 041702 (2020).
- [39] A. S. Solntsev and A. A. Sukhorukov, *Rev. Phys.* **2**, 19 (2017).
- [40] H. de Riedmatten, J. Laurat, C. W. Chou, E. W. Schomburg, D. Felinto, and H. J. Kimble, *Phys. Rev. Lett.* **97**, 113603 (2006).
- [41] See Supplemental Material at <http://link.aps.org/supplemental/10.1103/PhysRevLett.129.173602> for technical details and further discussion.
- [42] R. Micallef, Y. S. Kivshar, J. Love, D. Burak, and R. Binder, *Opt. Quantum Electron.* **30**, 751 (1998).
- [43] W. ge Song, H. Li, S. Gao, C. Chen, S. Zhu, and T. Li, *Adv. Opt. Photonics* **2**, 1 (2020).
- [44] M. M. Dignam and C. M. de Sterke, *Phys. Rev. Lett.* **88**, 046806 (2002).
- [45] J. B. Spring, P. S. Salter, B. J. Metcalf, P. C. Humphreys, M. Moore, N. Thomas-Peter, M. Barbieri, X.-M. Jin, N. K. Langford, W. S. Kolthammer, M. J. Booth, and I. A. Walmsley, *Opt. Express* **21**, 13522 (2013).
- [46] A. M. Fox, M. Fox *et al.*, *Quantum Optics: An Introduction* (Oxford University Press, New York, 2006), Vol. 15.
- [47] M. O. Scully and M. S. Zubairy, *Am. J. Phys.* **67**, 648 (1999).
- [48] J. M. Zeuner, N. K. Efremidis, R. Keil, F. Dreisow, D. N. Christodoulides, A. Tünnermann, S. Nolte, and A. Szameit, *Phys. Rev. Lett.* **109**, 023602 (2012).
- [49] J. Arrazola, V. Bergholm, K. Brádler, T. Bromley, M. Collins, I. Dhand, A. Fumagalli, T. Gerrits, A. Goussev, L. Helt *et al.*, *Nature (London)* **591**, 54 (2021).